ORIGINAL ARTICLE

Participation of GATA-3 in regulation of bone healing through transcriptional upregulation of *bcl-x$_L$* expression

Mei-Hsiu Liao[1], Pei-I Lin[1], Wei-Pin Ho[2,3], Wing P Chan[2,4], Ta-Liang Chen[5] and Ruei-Ming Chen[1,2,5]

We have previously demonstrated the expression of GATA-DNA-binding protein (GATA)-3, a transcription factor, in osteoblasts and have verified its function in transducing cell survival signaling. This translational study was further designed to evaluate the roles of GATA-3 in regulating bone healing and to explore its possible mechanisms. A metaphyseal bone defect was created in the left femurs of male ICR mice. Analysis by micro-computed topography showed that the bone volume, trabecular bone number and trabecular thickness were augmented and that the trabecular pattern factor decreased. Interestingly, immunohistological analyses showed specific expression of GATA-3 in the defect area. In addition, colocalized expression of GATA-3 and alkaline phosphatase was observed at the wound site. As the fracture healed, the amounts of phosphorylated and non-phosphorylated GATA-3 concurrently increased. Separately, GATA-3 mRNA was induced during bone healing, and, levels of Runx2 mRNA and protein were also increased. The results of confocal microscopy and co-immunoprecipitation showed an association between nuclear GATA-3 and Runx2 in the area of insult. In parallel with fracture healing, Bcl-XL mRNA was significantly triggered. A bioinformatic search revealed the existence of a GATA-3-specific DNA-binding element in the promoter region of the *bcl-x$_L$* gene. Analysis by chromatin immunoprecipitation assays further demonstrated transactivation activity by which GATA-3 regulated *bcl-x$_L$* gene expression. Therefore, this study shows that GATA-3 participates in the healing of bone fractures via regulating *bcl-xL* gene expression, owing to its association with Runx2. In the clinic, GATA-3 may be used as a biomarker for diagnoses/prognoses or as a therapeutic target for bone diseases, such as bone fractures.

INTRODUCTION

Bone fractures are common accidents that occur worldwide. A broken bone usually leads to acute or chronic pain, movement problems, a decreased quality of life, and even death.[1] Osteoporosis-induced bone fractures are a severe complication because they heal with difficulty and are commonly associated with increased morbidity and mortality.[2] Clinically, the standard treatment for bone fractures is to set the broken bone in place to allow it to heal properly. At the same time, surgeons may prescribe certain medications, such as acetaminophen or ibuprofen, to decrease inflammation and subsequent pain.[3] However, at present, no effective drug is available to effectively improve fracture healing. The key step in discovering new medications or new strategies for therapy of bone fractures is to elucidate the detailed mechanisms of bone healing. Fracture healing is characteristically distinguished by four stages: an

inflammatory response, soft callus formation, hard callus formation and bone remodeling.[4] A variety of osteogenesis-related cells, such as mesenchymal cells, osteoprogenitor cells, osteoblasts, osteoclasts and chondrocytes, are involved in the overlapping progression of bone healing.[5,6] Among them, osteoblasts play a crucial role in bone formation and remodeling.

Bone structure is maintained by bone remodeling, a dynamically balanced process of osteoblast-mediated bone formation and osteoclast-involved bone resorption.[7] When a bone breaks, the tight cellular and molecular controls of bone remodeling are consecutively disrupted. Fracture-induced inflammatory responses, including low-oxygen tension, impaired perfusion, cell migration and the release of active molecules, are predominant initiating factors that directly affect the primary outcomes of fracture management and

[1]Graduate Institute of Medical Sciences, College of Medicine, Taipei Medical University, Taipei, Taiwan; [2]Cell Physiology and Molecular Image Research Center, Taipei Medical University-Wan Fang Medical Center, Taipei, Taiwan; [3]Department of Orthopedic Surgery, Taipei Medical University-Wan Fang Medical Center, Taipei, Taiwan; [4]Department of Radiology, Wan Fang Hospital, Taipei Medical University, Taipei, Taiwan and [5]Anesthesiology and Health Policy Research Center, Taipei Medical University Hospital, Taipei, Taiwan
Correspondence: Professor R-M Chen, Graduate Institute of Medical Sciences, Taipei Medical University, 250 Wu-Xing Street, Taipei 110, Taiwan.
E-mail: rmchen@tmu.edu.tw

restoration.[5] In general, a fracture can spontaneously repair itself after appropriate therapy. Nevertheless, multiple arrays of intrinsic and extrinsic factors may interfere with the healing of a broken bone.[8] For example, osteoblast recruitment to the site of a broken bone plays vital roles in skeletal repair, development and remodeling.[9] Unfortunately, a complicated network of systemic and local inflammatory events can suppress osteoblast differentiation, growth, and activities, thus obstructing osteoblast enrollment at injured sites and subsequently retarding bone repair.[4,5] Bai *et al.* have reported that reactive oxygen species induced by fracture-involved inflammation can cause osteoblast dysfunction and disrupt bone repair and remodeling, owing to the induction of osteoblast dysfunction or death.[10] Moreover, our previous studies have also reported that the overproduction of nitric oxide (NO) from inflammatory responses induces apoptotic insult to osteoblasts via modulating the expression of apoptosis-related Bax and Bcl-2.[11,12] Consequently, decreasing the disruption of osteoblast activities by these inflammation-related factors would be helpful in improving bone healing and remodeling.

GATA-DNA-binding proteins (GATAs), a family of transcriptional regulators with two zinc finger motifs, control cell activity through binding to the nucleotide sequence element (A/T)GATA(A/G) and regulating the expression of certain genes.[13] GATA-1–3 regulate critical events in hematopoietic lineages, whereas GATA-4–6 have been reported to mainly be expressed by non-hematopoietic tissues.[14] However, our previous study first demonstrated GATA-3 expression in non-hematopoietic bone cells, and showed that this transcriptional factor functions as a transducer that mediates survival signals in osteoblasts.[15] Regarding the mechanism, previous studies have shown that phosphorylation of GATA-3 by various kinases, including p38 mitogen-activated protein kinase (MAPK), cyclin-dependent kinase 2 or AKT serine/threonine kinase 1, may play an essential role in regulating the development and differentiation of Th2 cells, T cells and natural helper cells.[16–19] In addition, Meijome *et al.* have reported that a GATA-1 deficiency is beneficial for the formation of trabecular bone in osteoprotegerin-knockout mice.[20] Recently, we have further found that GATA-5 protects against oxidative stress-induced apoptotic insult to osteoblasts.[21] Hence, GATAs are expressed in osteoblasts and participate in controlling osteoblast survival and functions. Runt-related transcription factor 2 (Runx2) is another transcription factor that regulates osteoblast growth and differentiation.[22,23] In response to the regulation of programmed cell death, Bcl-X_L, one of the Bcl-2 members with homology to BH1–3, is an antiapoptotic protein that associates with apoptotic Bax and subsequently prevents mitochondrial disruption and cytochrome C release.[24] Previous results from our lab have shown that the transactivation activity of GATA-3 in osteoblasts occurs through association with Runx2 to stimulate *bcl-x_L* gene expression.[15] Osteoblast-mediated bone formation participates in bone fracture repair. Nevertheless, the roles of GATA-3 in bone healing remain unknown. Therefore, in this study, we evaluated the roles of GATA-3 in fracture healing and the possible underlying mechanisms by using a metaphyseal defect model of mouse femurs.

MATERIALS AND METHODS
Animal model of bone defects
Male ICR mice (25–30 g) were purchased from the Animal Center of the College of Medicine, National Taiwan University (Taipei, Taiwan). All procedures were performed according to the National Institutes of Health Guidelines for the Use of Laboratory Animals and were approved (no: WAN-LAC-100-013) by the Institutional Animal Care and Use Committee of Taipei Medical University-Wan Fang Hospital (Taipei, Taiwan). Animals were allowed to acclimate for 1 week in their animal quarters under air conditioning and an automatically controlled photoperiod of 12 h of light daily.

After bone fracture, mesenchymal stem cells and osteochondral progenitors derived from the bone marrow, cortex, periosteum and surrounding soft tissues were stimulated by growth factors and certain mediators, such as Runx2, and were then differentiated into osteoblasts.[4,25] In this study, a metaphyseal bone defect of the femur was created according to a previously described method.[26] Briefly, mice were anesthetized with an intraperitoneal injection of chloral hydrate (350 mg kg^{-1} body weight). A metaphyseal bone defect of 1.0 mm in diameter was created in the left proximal femur by drilling through the anterolateral cortical bone into the metaphyseal cancellous bone to the opposite cortex (with a depth of ~ 2 mm). The right femur served as a sham group. The surgical wound was sewn up with 4.0 nylon sutures. Animals were allowed free unrestricted weight bearing after recovery from anesthesia. Body weights were measured after surgery.

Micro-computed tomographic (μCT) analysis
Bone healing was evaluated using μCT as described previously.[27] At 1, 3, 5 and 7 days after the bone defect had been created, the mice were killed, and the femurs were collected. After removal of the muscle and connective tissues, the femurs were weighed and photographed. The μCT analysis was conducted using a Skyscan 1076 μCT scanner (Skyscan, Antwerp, Belgium). The formation of soft calluses, trabecular bone and mineral calluses was scanned, observed or quantified using the μCT scanner (Skyscan). The scanning axis nominally coincided with the diaphyseal axis of the control femur. The femurs with a bone defect were scanned using the same parameters (9 μm per slice, 50 kV, 140 μA, 0.5-mm Al filter and a 3300-ms exposure time). High-resolution images of the femurs were generated in a 3D polygonal resampling using Skyscan 3D-Creator software (Skyscan), and morphometric parameters were calculated for trabecular bone regions of interest using a Skyscan CT-Analyser (Skyscan).

Histological analysis
Histological analyses of the femurs were conducted as described previously.[28] After the bone defects were created, animals werekilled, and the femurs were collected and cleaned. The femurs were fixed in 4% formaldehyde, decalcified, dehydrated, embedded in paraffin wax and sliced into 5-μm sections. Before staining, xylene and ethanol gradients were used for deparaffinization and rehydration. The slices were stained with hematoxylin and eosin (H&E). All specimens were observed and photographed using a light microscope (Nikon, Tokyo, Japan).

Confocal microscopic analyses of GATA-3, alkaline phosphatase (ALP), and Runx2 expression and co-localization

The expression of GATA-3, ALP and Runx2 in the bone defect area was analyzed using confocal microscopy, as described previously.[29] After creation of the bone defect, mice were killed, and the femurs were collected. After removal of the muscle and connective tissue, the bone samples were fixed, decalcified, embedded in paraffin wax, and sliced. Immunodetection of GATA-3, ALP and Runx2 in the femurs was carried out at 4 °C overnight using a mouse monoclonal antibody (mAb) against human GATA-3 (Santa Cruz Biotechnology, Santa Cruz, CA, USA), a rabbit polyclonal antibody (pAb) against mouse Runx2 and a rabbit pAb against human ALP (Abcam, Cambridge, UK), respectively. After being washed, the slices were sequentially reacted with the secondary antibody and biotin-SP-conjugated Affini-Pure anti-mouse immunoglobulin G (IgG) (Jackson ImmunoResearch, West Grove, PA, USA) at room temperature for 1 h. After the second wash, the third antibody with Cy3-conjugated streptavidin (Jackson ImmunoResearch) was added to the femur slice and allowed to react at room temperature for 30 min. Nuclear DNA was stained with 4′,6-diamidino-2-phenylindole (DAPI). A confocal laser scanning microscope (model FV500, Olympus, Tokyo, Japan) was utilized for sample observation. The excitation wavelength was set to 568 nm, and a 585-nm long-pass filter was used to collect the emitted light. Images were acquired and quantified using FLUOVIEW software (version 4.0, Olympus). In a section, the densities of the merged signals within three different ROIs were chosen and analyzed. The average density of the positive signals was the average of the values for 1–3 sections in each group.

Reverse-transcription polymerase chain reaction (RT-PCR)

The expression of GATA-3, Runx2, and Bcl-X_L messenger RNA (mRNA) in the bone defect sites were determined using RT-PCR analyses, as described previously.[30] After creation of the bone defect, mice werekilled, and the femurs were collected and cleaned. Total RNAs from control and bone defect sites were prepared for analyses of GATA-3, Runx2, Bcl-X_L and β-actin mRNA. Oligonucleotide primers were designed and synthesized by Mission Biotechnology (Taipei, Taiwan). The oligonucleotide sequences of the respective upstream and downstream primers were 5′-TACTTGCGTTTTTCGCAGGA-3′ and 5′-GCGTCCTTCATGCCTTTCT-3′ for GATA-3 mRNA;[15] 5′-GACAGAAGCTTGATGACTCTAAACC-3′ and 5′-CTGTAAT CTGACTCTGTCCTTGTG-3′ for Runx2 mRNA;[12] 5′-TCGAAGAG AATAGGACTGAG-3′ and 5′-TCAAAGCTCTGATACGCGGT-3′ for mouse Bcl-X_L mRNA;[15] and 5′-GTGGGCCGCCCTAGGCACCAG-3′ and 5′-CTCTTTGATGTCACGCACGATTTC-3′ for β-actin mRNA.[15] PCR products were loaded onto a 1.8% agarose gel containing 0.1 µg ml^{-1} ethidium bromide and were electrophoretically separated. DNA bands were visualized and photographed under ultraviolet-light exposure. Intensities of the DNA bands in the agarose gel were quantified with the aid of a digital imaging system (UVtec, Cambridge, UK).

Immunoblotting analyses of GATA-3, phosphorylated (p) GATA-3, Runx2, Bcl-X_L, and β-actin

Protein analyses were carried out according to a previously described method.[31] After creation of the bone defect, mice werekilled, and the femurs were collected and cleaned. The femurs were frozen in liquid nitrogen and crushed. All samples were homogenized in radio-immunoprecipitation assay buffer (50 mM Tris–HCl at pH 7.4, 1% NP40, 0.25% sodium deoxycholate, 150 mM sodium chloride, 1 mM ethylene glycol tetraacetic acid, 1 mM phenyl methyl sulfonyl fluoride, 1 mM sodium orthovanadate and 5 µg ml^{-1} leupeptin). After centrifugation at 12 500 r.p.m. at 4 °C for 30 min, the supernatants were collected and quantified using a bicinchonic acid protein assay kit (Pierce, Rockford, IL, USA). Proteins (50 µg per well) were subjected to sodium dodecyl sulfate polyacrylamide gel electrophoresis (SDS–PAGE) and were transferred to nitrocellulose membranes. GATA-3, pGATA-3, Runx2 and Bcl-X_L were immunodetected using mouse mAbs or rabbit pAbs. Cellular β-actin protein was immunodetected using a mouse mAb against mouse β-actin (Sigma, St Louis, MO, USA) as the internal standard. These protein bands were quantified using a digital imaging system (UVtec).

Co-immunoprecipitation and immunoblotting assays

Co-immunoprecipitation and immunoblotting analyses were carried out using an ExtractCruz kit from Santa Cruz Biotechnology, as described previously.[15] After production of the bone defect, the mice were killed, and the femurs were collected and cleaned. The femurs were frozen in liquid nitrogen and crushed. All samples were homogenized in radioimmunoprecipitation assay buffer. After centrifugation at 12 500 r.p.m. at 4 °C for 30 min, the supernatants were collected and incubated with a rabbit pAb against human recombinant GATA-3 (Santa Cruz Biotechnology) and were subsequently incubated with protein A-Sepharose (50% slurry) at 4 °C overnight, then washed three times. The pellet was resuspended in the same volume of SDS sample buffer and was boiled to remove the Sepharose beads. Then, cell lysates and immunoprecipitates were analyzed by an immunoblotting assay of Runx2 using a rabbit pAb against mouse Runx2. Normal rabbit IgG purchased from Santa Cruz Biotechnology was used in the pull-down assay as the negative control.

Bioinformatic approach

A GATA-3-specific DNA-binding element in the promoter region of the bcl-xl gene was predicted using different bioinformatic systems, including TESS and PROMO.[32,33] Our results indicated that the GATA-3-binding site is located at − 471 to − 463 bp. The respective upstream and downstream primers for amplification of this GATA-3-specific DNA-binding element were 5′-CGTCTTATAGCCACCC CACC-3′ and 5′-CCCATGTGGGAACAGACACA-3′. PCR products were separated on a 1.8% agarose gel and were then isolated for DNA sequencing. The DNA sequence was confirmed, and the primers were used for chromatin immunoprecipitation (ChIP) assays.

ChIP assay

Binding of GATA-3 to its specific DNA elements in the promoter region of the bcl-x_L gene was determined with ChIP assays, as described previously.[34] After creation of the bone defect, mice were killed, and the femurs were collected and cleaned. The femurs were frozen in liquid nitrogen, crushed, and then homogenized in phosphate-buffered saline (PBS; 0.14 M NaCl, 2.6 mM KCl, 8 mM Na_2HPO_4, and 1.5 mM KH_2PO_4) containing protease inhibitors. The ChIP assay was performed with an Upstate EZ ChIP Kit (Millipore, Billerica, MA, USA) according to the manufacturer's protocol. Protein-DNA crosslinking was fixed with 1% formaldehyde for 20 min and stopped by glycerol. After centrifugation and washing, samples were lysed using SDS-lysis buffer (1% SDS, 10 mM EDTA, and 50 mM Tris, at pH 8.1). The lysates were sonicated into chromatin fragments (< 500 bp). Immunoprecipitation was performed with an antibody to GATA-3 (Santa Cruz Biotechnology). Rabbit IgG (Santa

Cruz Biotechnology) was used as an isotype control antibody. Chromatin antibody complexes were captured on protein G magnetic beads (Millipore). After being washed, DNA–protein cross-links were reversed at 65 °C overnight. The immunoprecipitated DNA was treated with RNase A and proteinase K and purified using the spin columns provided in a GeneJET Gel Extraction Kit (Thermo Fisher Scientific, Waltham, MA, USA). Input DNA was also purified using the spin columns (Thermo Fisher Scientific). The purified DNA and input genomic DNA were analyzed by PCR. The results of Bcl-X_L binding were normalized to the input DNA. The primers used for ChIP (PCR product length, 177 bp) were 5′-CGTCTTATAGCCACCCCACC-3′ and 5′-CCCATGTGGGAACAGACACA-3′. The PCR products were separated using electrophoresis on a 1.8% agarose gel. The input DNA was analyzed as the loading control. These DNA bands were quantified using a digital imaging system (UVtec).

Statistical analysis

The statistical significance of the differences between the sham and surgery-treated groups was evaluated using Duncan's multiple-range test. Statistical analyses between groups over time were carried out by a two-way analysis of variance (ANOVA). A *P* value of < 0.05 was considered statistically significant.

RESULTS

Bone healing after a bone defect

Healing of bone defects was analyzed using μCT after bone injury created in mouse femurs (Figure 1). One day after wound creation, trabecular bone was observed in the bone defect site (Figure 1a, left panel). The amounts of trabecular bone had increased by day 3 (left second panel). Five and seven days later, the amounts of trabecular bone and the bone volume had been noticeably increased (left third and fourth panels). Serial two-dimensional sections of the damaged area were scanned to further determine changes in the bone microenvironment (Figure 1b). The results indicated that soft calluses and trabecular bone had successively formed 1, 3, 5 and 7 days after creation of the bone defect. Furthermore, mineralized calluses had taken shape around the site of insult by day 7 (Figure 1b). Representative μCT three-dimensional images of trabecular bone are presented in Figure 1c. The data showed that bone formation considerably proceeded after bone damage had been created in the femur (Figure 1c).

At 3, 5 and 7 days after creation of the bone defect, the ratio of bone volume over total volume respectively increased by 2.3-, 4.8- and 6.4-fold compared with that of the 1-day-treated group (Figure 2a). Furthermore, numbers of trabecular bones were increased 3, 5 and 7 days after bone surgery (Figure 2b). At 5 and 7 days after the creation of the bone defect, the trabecular thickness significantly increased by 48% and 66%, respectively (Figure 2c). In comparison to the 1-day-treated animals, the animals that were killed for 3, 5 and 7 days after creation of the bone defect showed 30%, 52% and 67% decreases in the trabecular pattern factor, respectively (Figure 2d).

Specific expression and colocalization of GATA-3 and ALP in the bone defect site

The expression and colocalization of GATA-3 and ALP were assayed to determine the source of GATA-3 in the defect area (Figure 3). Three days after the bone insult, the left femur was sliced in a coronal section and stained with H&E (Figure 3a, top panel). Moreover, an immunohistological analysis of GATA-3 was carried out (bottom panel). The results revealed that GATA-3 was specifically produced in the bone wound area, but not in proximal, middle or distal metaphysic areas. Confocal microscopy analyses further demonstrated the increase of GATA-3 in the damaged site (Figure 3b). The amounts of ALP also increased in the same area. Interestingly, the results of confocal microscopy showed the colocalization of GATA-3 and ALP in the nucleus during bone healing (Figure 3b).

Induction of GATA-3 gene expression during bone healing

RNA and protein analyses were performed to determine the mechanisms of GATA-3 expression during bone healing (Figure 4). In the sham group, low levels of GATA-3 and pGATA-3 were detected (Figure 4a, top panel, lane 1). However, 1 day after creation of the bone defect, the amounts of GATA-3 and pGATA-3 had clearly increased in the defect area (lane 2). After 3, 5 and 7 days, the levels of GATA-3 and pGATA-3 were increased. β-actin was immunodetected as the internal control (bottom panel). These protein bands were quantified and statistically analyzed (Figure 4b). Compared with those in the sham group, the amounts of GATA-3 were elevated 6.4-, 8.6-, 5.6- and 6.3-fold at 1, 3, 5 and 7 days, respectively, after creation of the bone defect. Simultaneously, the amounts of pGATA-3 were also increased by 4.9-, 11.4-, 6.1- and 7.2-fold on days 1, 3, 5 and 7, respectively (Figure 4b).

The results of RNA analyses indicated low levels of GATA-3 mRNA in the sham group (Figure 4c, top panel, lane 1). In contrast, GATA-3 mRNA was massively induced 1 day after creation of the bone defect (lane 2). The amounts of GATA-3 mRNA clearly increased at 3, 5 and 7 days after creation of the bone defect (lanes 3–5). Expression of β-actin mRNA was analyzed as the internal control (bottom panel). These DNA bands were quantified and statistically analyzed (Figure 4d). At 1, 3, 5 and 7 days after creation of the bone defect, the levels of GATA-3 mRNA were respectively increased by 150%, 180%, 73% and 103%.

Runx2 gene expression during bone healing

Because Runx2 plays a crucial role in osteogenesis, its gene expression in bone healing was investigated (Figure 5). In the sham group, low levels of Runx2 protein were detected (Figure 5a, top panel, lane 1). In contrast, the amounts of Runx2 protein were clearly elevated in the bone insult site 1 day after creation of the bone defect (lane 2). In comparison, Runx2 protein levels were elevated on days 3, 5 and 7 (lanes 3–5). The amounts of β-actin were analyzed as the internal control (bottom panel). These immunorelated protein bands were quantified and statistically analyzed (Figure 5b). At
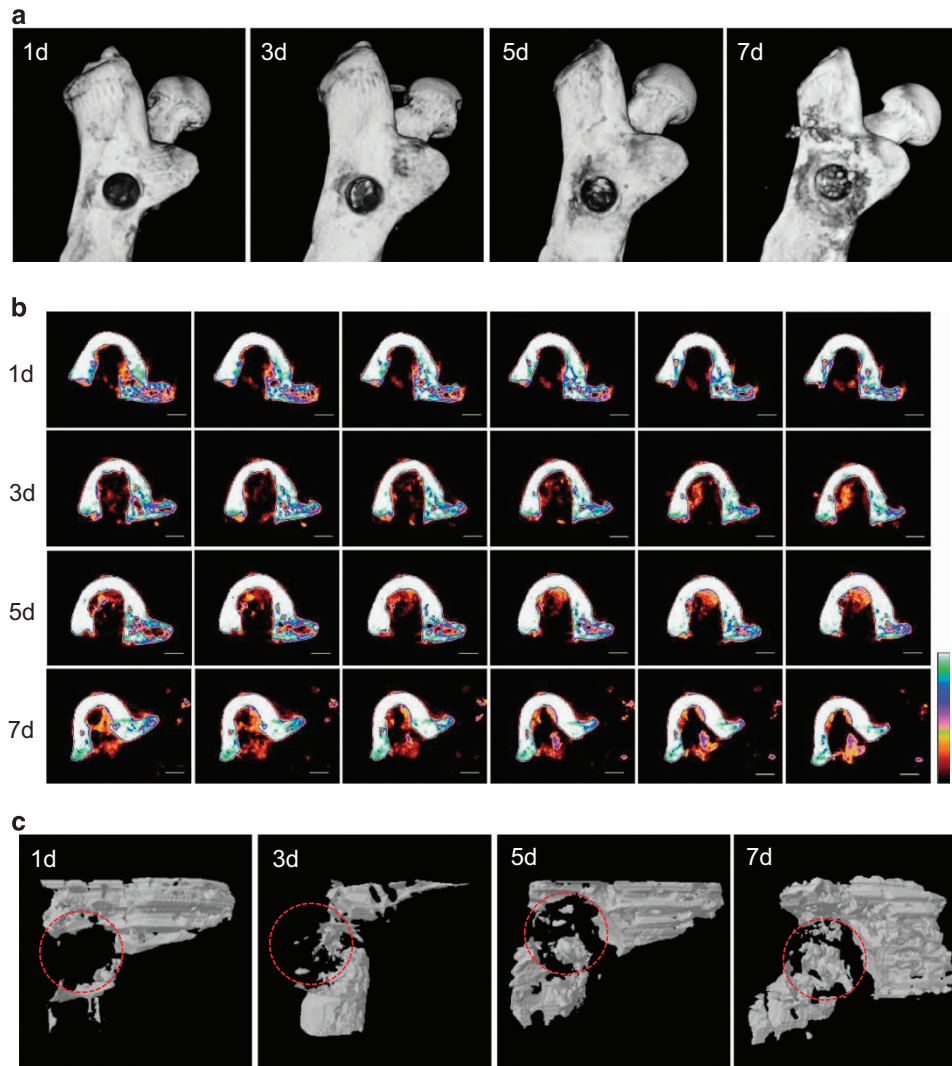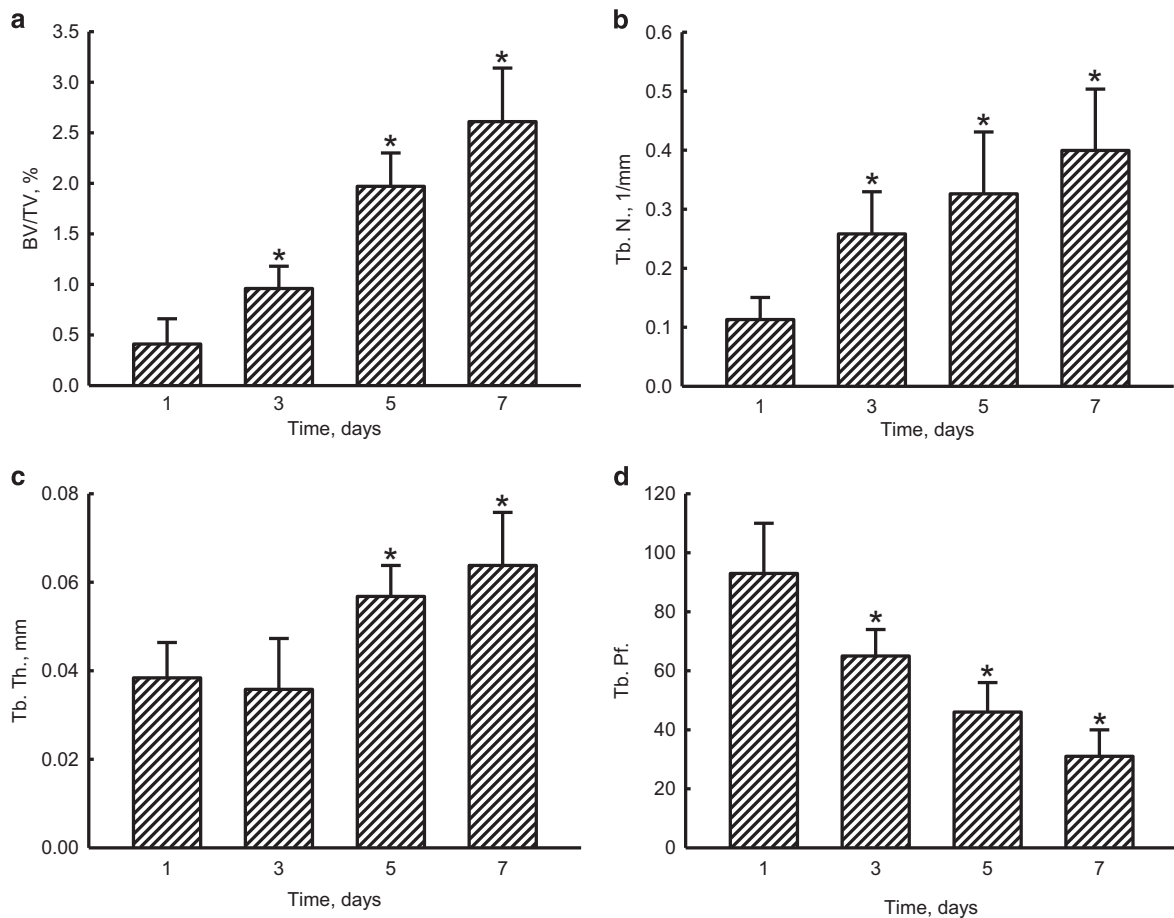
Figure 1 Bone healing after a bone defect. Male ICR mice were anesthetized, and a metaphyseal bone defect was created in the left proximal femurs. The right femurs were treated as the sham group. At 1, 3, 5 and 7 days after surgery, animals were killed, and the femurs were collected for analysis by micro-computed topography (μCT). Representative three-dimensional μCT images of the bone defect area in the proximal femurs are shown (**a**). Serial two-dimensional sections of mineralized calluses in the defect sites were scanned and are shown (**b**). Production of trabecular bone in the insulted sites was also analyzed and is shown (**c**). For each group, a representative image selected from four animals from four independent experiments is shown.

1, 3, 5 and 7 days after creation of the bone defect, the levels of Runx2 protein significantly increased by 2.1-, 1.9-, 3.2- and 3.5-fold, respectively.

RNA analyses additionally revealed that Runx2 mRNA was detectable in the sham group (Figure 5c, top panel, lane 1). In contrast, Runx2 mRNA was notably induced in the wound site of the femur 1 day after the bone defect was created (lane 2). Expression of Runx2 mRNA was also detected on days 3 and 5 (lanes 3 and 4). However, expression of Runx2 mRNA had returned to the basal level by day 7 (lane 5). β-actin mRNA was analyzed as the internal control (bottom panel). The DNA bands were quantified and statistically analyzed (Figure 5d). At 1, 3, and 5 days after creation of the bone defect, the amounts of Runx2 mRNA had been induced by 2.8-, 3.1- and 2.3-fold, respectively.

Association between nuclear GATA-3 and Runx2 during bone healing

The translocation and colocalization of GATA-3 and Runx2 were further analyzed to determine the mechanisms of GATA-3's involvement in bone healing (Figure 6). Image analyses by confocal microscopy showed levels of GATA-3 and Runx2 in the damaged area at 1, 3, 5 and 7 days after creation of the bone defect (Figure 6a, top first and second panels). Nuclei were stained with DAPI (top third panel). Merged signals showed the colocalization of GATA-3 and Runx2 in nuclei (bottom panels). These merged signals were quantified and statistically analyzed (Figure 6b). At 1, 3, 5 and 7 days after creation of the bone defect, the colocalization of nuclear GATA-3 and Runx2 had increased by 22-, 13-, 9- and 14-fold, respectively.

Figure 2 Quantitative analysis of trabecular bone in the bone defect area by micro-computed topography (μCT). Male ICR mice were anesthetized, and a metaphyseal bone defect was created in the left proximal femurs. The right femurs were treated as the sham group. At 1, 3, 5 and 7 days after surgery, animals were killed, and the femurs were collected. The bone formation in regions of interest was analyzed by μCT for trabecular bone volume (BV) per total volume (TV) (**a**), trabecular thickness (Tb. Th.) (**b**), trabecular number (Tb. N.) (**c**), and trabecular pattern factor (Tb. Pf.) (**d**). Each value represents the mean ± s.d. for $n = 4$. * Values significantly differ from those of the 1-day-treated group, $P < 0.05$. d, day.

The translocation and colocalization of GATA-3 and Runx2 were further identified by a co-immunoprecipitation assay (Figures 6c and d). At 1, 3, 5 and 7 days after the bone defect was created in the left femur, the levels of Runx2 in the immunoprecipitates prepared against the GATA-3 antibody had clearly increased compared with the levels in the sham group (Figure 6c, top panel, lanes 1–5). In comparison, the amounts of p-GATA-3 in the anti-Runx2 immunoprecipitates had increased 1, 3, 5 and 7 days after creation of the bone defect (middle panel, lanes 1–5). However, the levels of GATA-3 were not altered (lanes 1–5). The amounts of the IgG heavy chain were determined as the internal standard (bottom panel). The association of GATA-3 and Runx2 in osteoblasts was assayed as a positive control (lane 6). Mouse normal IgG was used as a negative control (lane 7). Runx2 and GATA-3 were detected (lane 8). The co-immunoprecipitated protein bands were quantified and statistically analyzed (Figure 6d). At 1, 3, 5 and 7 days after creation of the bone defect, the levels of Runx2 were respectively increased by 1.7-,

2-, 1.9- and 3.1-fold. In contrast, the amounts of p-GATA-3 had increased by 2-, 3-, 2.8- and 2.9-fold, respectively (Figure 6d).

GATA-3-mediated regulation of bcl-x$_L$ gene expression during bone healing

The regulation of *bcl-X$_L$* gene expression by GATA-3 was examined to determine how this transcription factor participates in bone healing (Figure 7). In the sham group, limited levels of Bcl-X$_L$ mRNA were detected (Figure 7a, top panel, lane 1). In contrast, the expression of Bcl-X$_L$ mRNA in bone defect sites was induced at 1, 3, 5 and 7 days after creation of the bone defect (lanes 2–5). β-actin mRNA was analyzed as the internal control (bottom panel). These DNA bands were quantified and statistically analyzed (Figure 7b). At 1, 3, 5 and 7 days after bone defect surgery, the levels of Bcl-X$_L$ mRNA in the bone defect site were respectively induced 7-, 10-, 6- and 8-fold.
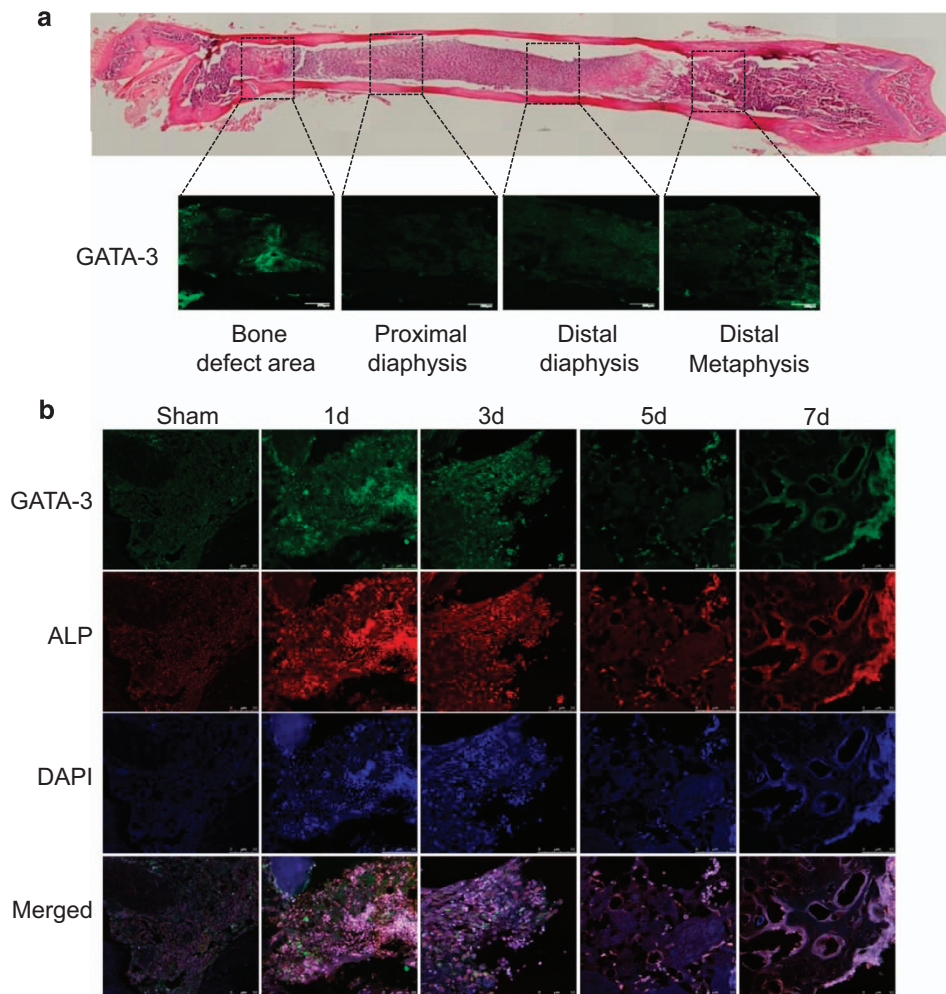
Figure 3 Specific expression of GATA-3 in the bone defect area and its colocalization with alkaline phosphatase (ALP) during bone healing. Male ICR mice were anesthetized, and a metaphyseal bone defect was created in the left proximal femurs. The right femurs were treated as the sham group. To determine the differential expression of GATA-3 in normal and bone defect sites, animals were killed at day 3 after surgery, and the left femurs were collected and sliced in coronal sections. The femoral structure was stained with hematoxylin and eosin (**a**, top panel). Each femur was divided into the defect area, proximal diaphysis, middle diaphysis, and distal metaphysis and subjected to an immunohistological analysis of GATA-3 using confocal microscopy (bottom panel). The co-localization of GATA-3, ALP and nuclei (DAPI) in the bone defect site at 1, 3, 5 and 7 days after surgery was analyzed using confocal microscopy (**b**). For each group, a representative image selected from four animals from four independent experiments is shown. d, day. (**a**), ×200; (**b**), ×600.

A bioinformatic search showed the existence of a GATA-3-specific binding element in the 5′-promoter region (−463 to −471 base pairs) of the $bcl-x_L$ gene (Figure 7c). The results from ChIP assays revealed low levels of GATA-3 binding to the $bcl-X_L$ gene in the sham group (Figure 7d, top panel, lane 1). One day after creation of the bone defect, the binding of GATA-3 to the promoter region had increased (lane 2). After 3 and 7 days, the binding of GATA-3 to the promoter region of the $bcl-x_L$ gene had further increased in the bone defect site (lanes 3 and 4). Normal mouse IgG was used as a negative control (lane 5). The input was loaded as the internal control (bottom panel). These DNA bands were quantified and statistically analyzed (Figure 7e). At 1, 3 and 7 days after creation of the bone defect, the binding of GATA-3 to the specific DNA element had respectively increased by 47%, 48% and 82%.

DISCUSSION

GATA-3 participates in bone healing. After creation of a bone defect, trabecular and cortical bone formed in the wounded area. In parallel with bone healing, the levels of GATA-3 were specifically enhanced in the defect site. The recruitment of osteoblasts into the breakage site plays a vital role in fracture healing.[9] Our present results revealed augmented expression of ALP, a biomarker of osteoblasts, in the area of insult. Interestingly, confocal microscopic results demonstrated the colocalization of GATA-3 and ALP in the bone defect area. As a result, GATA-3 is expressed in recruited osteoblasts, and it then contributes to the process of bone healing. Previous studies have reported that bone fracture-induced inflammation is an initiating factor that causes osteoblast injury and consequent interruption of fracture restoration.[5,35] In contrast, the upregulation of Bcl-X_L, an antiapoptotic protein, protects

a

b

c

d
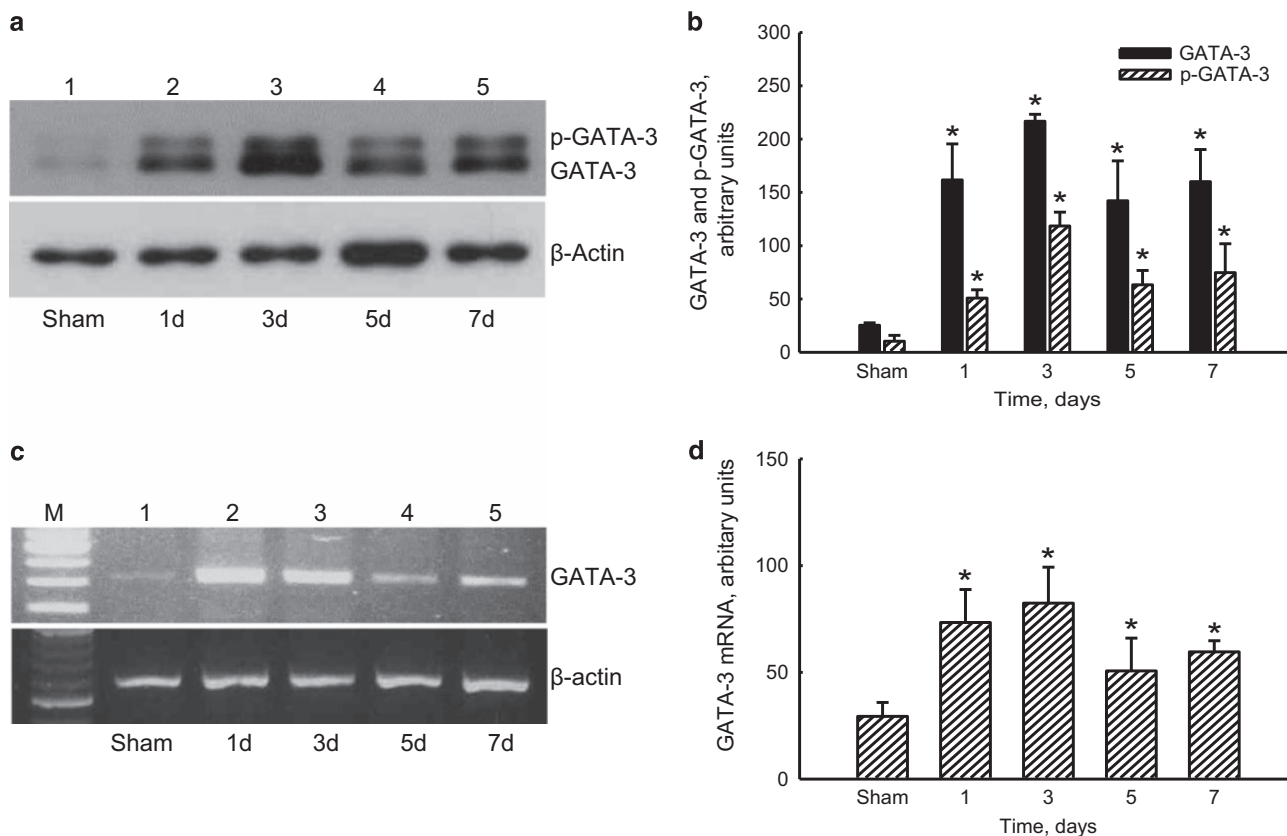
Figure 4 Induction of GATA-3 mRNA and protein expression during bone healing. Male ICR mice were anesthetized, and a metaphyseal bone defect was created in the left proximal femurs. The right femurs were treated as the sham group. At 1, 3, 5 and 7 days after surgery, the femurs were collected for RNA and protein analyses. Amounts of GATA-3 and phosphorylated (p)GATA-3 were immunodetected (**a**, top panel). β-actin was assayed as the internal standard (bottom panel). These immunorelated protein bands were quantified and statistically analyzed (**b**). Levels of GATA-3 mRNA were analyzed using a reverse-transcription polymerase chain reaction (**c**, top panel). β-actin mRNA was measured as the internal standard (bottom panel). These DNA bands were quantified and statistically analyzed (**d**). Each value represents the mean ± s.e.m. for $n = 6$. * Values significantly differ from the respective control group, $P < 0.05$. d, day.

osteoblasts from inflammation- or oxidative stress-induced cell death.[24,36] In this study, we demonstrated the induction of *bcl-x$_L$* gene expression during bone healing. Remarkably, the results from the CHIP assays showed that the transactivation activity of GATA-3 regulated *bcl-x$_L$* gene expression. Our previous study has shown the roles of GATA-3 in transducing survival signals in osteoblasts against oxidative stress-induced apoptotic insults via the upregulation of *bcl-x$_L$* gene expression.[15] This translational study further provides *in vivo* animal data demonstrating the functional roles of GATA-3 in bone repair. At present, no effective drug has been successfully developed for bone fracture therapy. Our present findings suggest the possibility of *de novo* therapeutic strategies for bone diseases using GATA-3 as a potential target.

The present animal model of bone defects provides a simple and standard model for investigating the mechanisms of bone healing. A metaphyseal defect model of the murine femur was used in this study to evaluate the mechanisms of bone healing. This is a reproducible bone defect model that offers a standardized environment for studies on the induction and remodeling of new trabecular bone in normal and genetically engineered mice.[26] Fracture healing is characterized into four

overlapping stages, including the inflammatory response, soft callus formation, hard callus production and bone remodeling.[4] In this study, soft tissues and woven bone were formed and observed using μCT at the beginning of fracture healing. Successively, trabecular bone, trabecular thickness, mineral calluses and bone volume increased. The trabecular pattern factor also decreased during bone healing. In addition, Uusitalo *et al.* have reported increased levels of osteogenesis-related gene expression, such as osteocalcin expression, throughout the healing period.[26] Our present results also indicated enhancements in the ALP protein and osteocalcin mRNA (data not shown). Accordingly, this metaphyseal defect model is an effective and reliable model for investigating the mechanics of fracture repair. In particular, trabecular bone was clearly formed and detected. Recently, a trabecular bone score has been suggested for application as a new complementary approach for osteoporosis evaluation.[37] This contemporary animal model can also be applied for assessment of the fracture risk induced by osteoporosis.

GATA-3 is specifically expressed by osteoblasts recruited to the bone defect site. A diverse set of osteogenesis-related cells, such as mesenchymal cells, osteoprogenitor cells, osteoblasts,
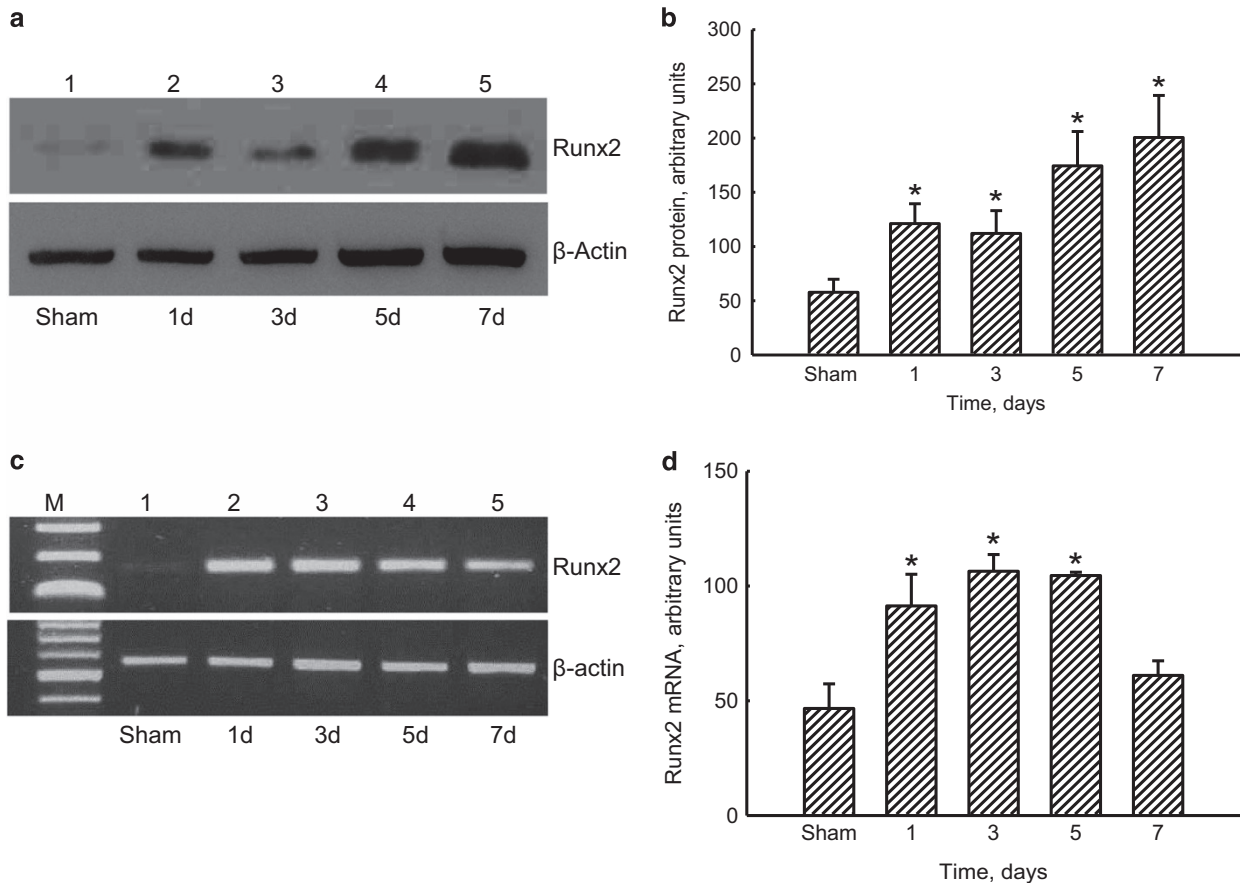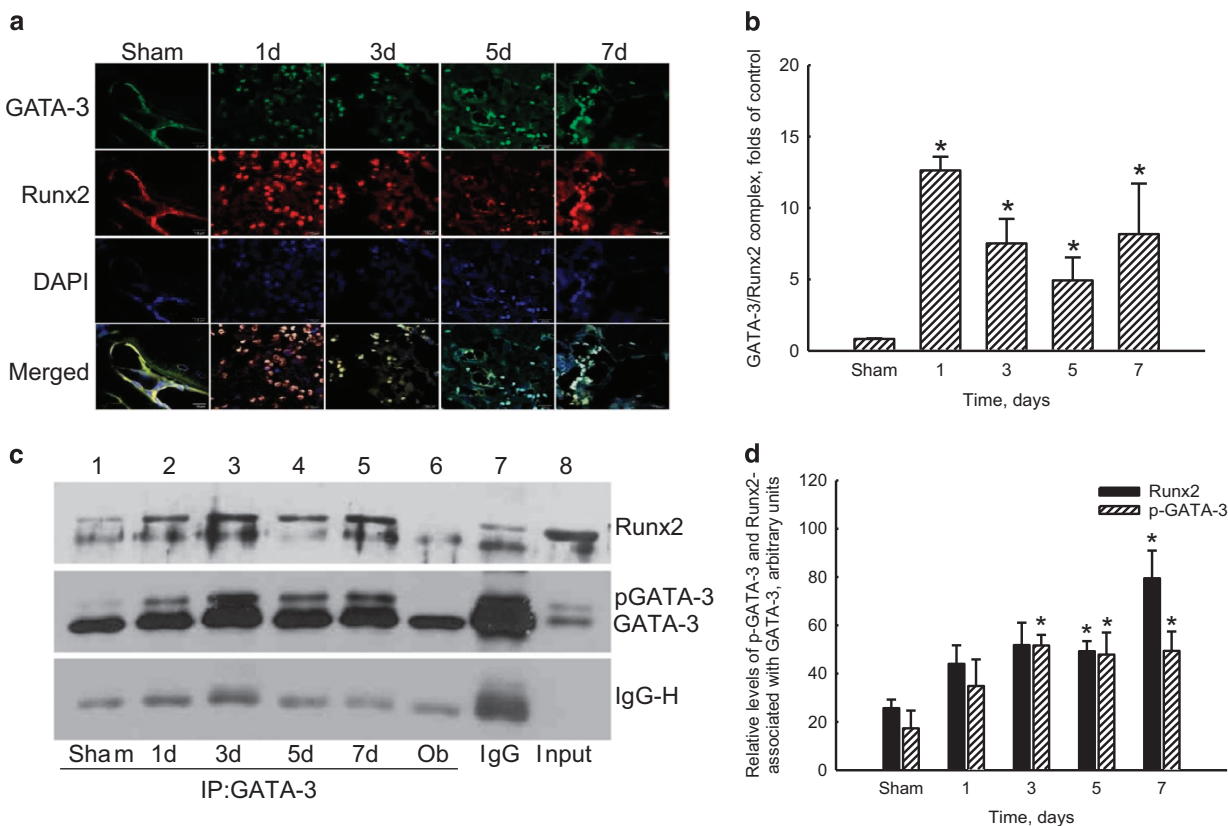
Figure 5 Induction of Runt-related transcription factor 2 (Runx2) mRNA and protein expression during bone healing. Male ICR mice were anesthetized, and a metaphyseal bone defect was created in the left proximal femurs. The right femurs were treated as the sham group. At 1, 3, 5 and 7 days after surgery, the femurs were collected for RNA and protein analyses. Amounts of Runx2 were immunodetected (**a**, top panel). β-actin was analyzed as the internal standard (bottom panel). These immunorelated protein bands were quantified and statistically analyzed (**b**). The amount of Runx2 mRNA was examined using a reverse-transcription polymerase chain reaction (**c**, top panel). β-actin mRNA was assayed as the internal standard (bottom panel). These DNA bands were quantified and statistically analyzed (**d**). Each value represents the mean ± s.e.m. for $n = 6$. * Values significantly differ from the respective control group, $P < 0.05$. d, day.

osteoclasts and chondrocytes, are involved in the overlapping processes of bone healing.[5,6] Osteoblast recruitment is generally thought to play crucial roles in bone repair and remodeling.[7,9] Our confocal microscopy imaging data showed the expansion of ALP-positive cells in the wounded area. ALP is a typical biomarker of osteoblasts.[38] Hence, osteoblasts essentially make a regular contribution to the construction of fracture repair via ensconcing themselves in the defect area. Compared with proximal, middle and distal diaphysis of the mouse femur, GATA-3 was specifically detected in the area of bone insult. In parallel with bone healing, the levels of GATA-3 were significantly elevated. Thus, these results present a meaningful line of evidence for the role of GATA-3 in fracture healing rather than bone remodeling. Typically, GATA-3 is considered to explicitly regulate cellular events in hematopoietic lineages.[14] Our previous study was the first report of the expression of GATA-3 by non-hematopoietic osteoblasts.[15] In the present study, our confocal microscopic images revealed colocalized expression of GATA-3 and ALP in the defect area, and the levels of colocalized GATA-3 and ALP simultaneously increased during the process of fracture repair. Our *in vitro* and *in vivo* results both demonstrated the expression of GATA-3 by osteoblasts. GATA-3 can transduce survival signals that protect osteoblasts from oxidative stress-induced apoptotic insult.[15] In contrast, the present study also validates the contribution of GATA-3 to the regulation of bone healing.

GATA-3 gene expression is sequentially induced during bone healing. The levels of GATA-3 in the bone defect site were increased. In parallel, the expression of GATA-3 mRNA was also induced. A previous study has reported the induction of GATA-3 mRNA and protein in osteoblasts.[15] Hence, bone healing may induce GATA-3 mRNA and protein expression by osteoblasts at the transcriptional level. Interestingly, the present study showed increases of phosphorylated GATA-3 during the healing of bone fractures. Chen *et al.* have reported that after phosphorylation by p38 MAPK, pGATA-3 regulates interleukin (IL)-5 and IL-13 gene expression by Th2 cells.[16] Moreover, Furusawa *et al.* have also shown the phosphorylation of GATA-3 by p38 MAPK in natural helper cells.[17] During the progression of bone healing, serial inflammatory responses are
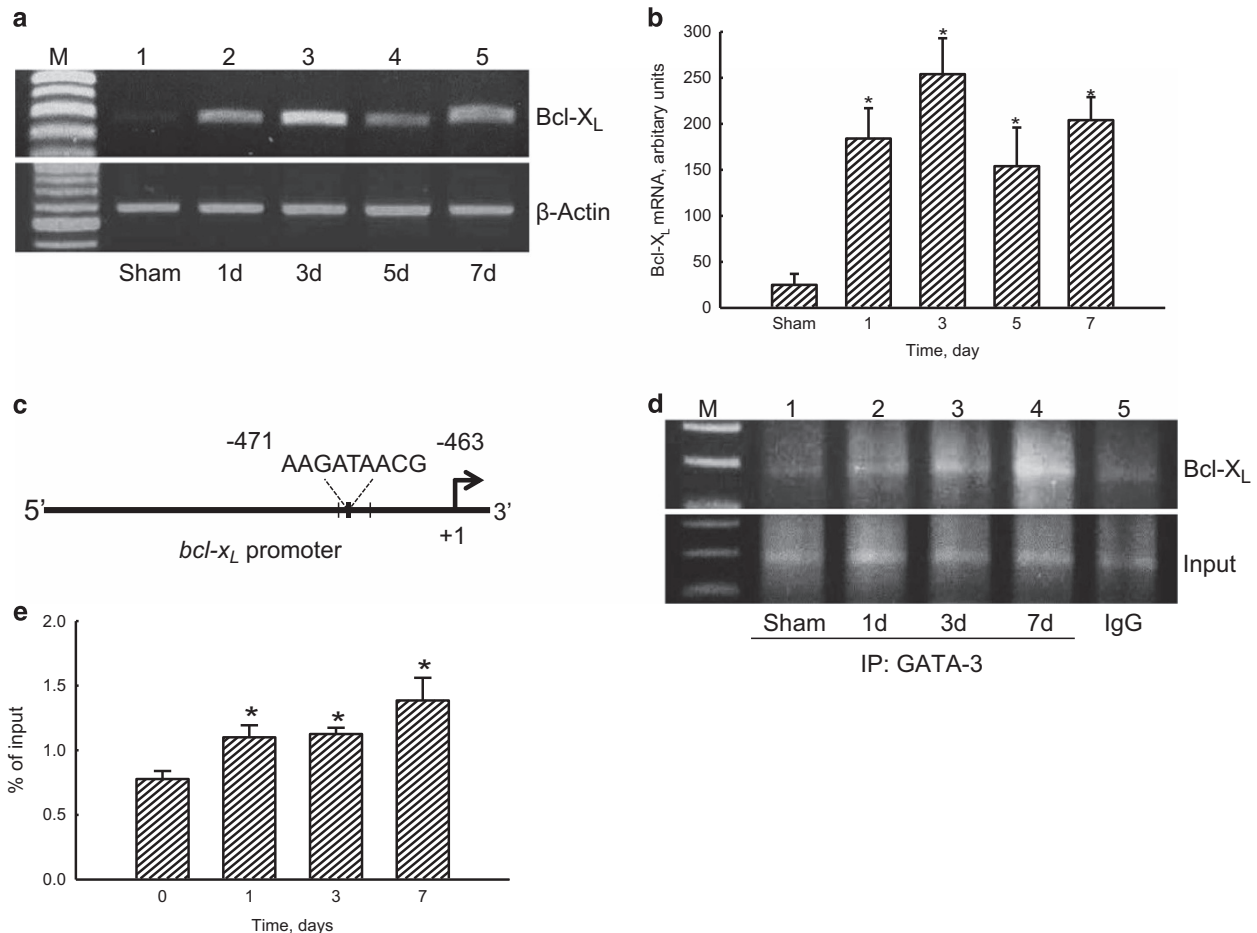
Figure 6 Association of nuclear GATA-3 and Runt-related transcription factor 2 (Runx2) during bone healing. Male ICR mice were anesthetized, and a metaphyseal bone defect was created in the left proximal femurs. The right femurs were treated as the sham-operated group. At 1, 3, 5, and 7 days after surgery, the femurs were collected and cleaned. The expression of GATA-3 (green signals) and Runx2 (red signals) in the bone defect sites were analyzed using confocal microscopy (**a**). Nuclei were stained with DAPI (blue signals). The association of nuclear GATA-3 and Runx2 (white signals) was observed, quantified and statistically analyzed (**b**). The complex of GATA-3 associated with Runx2 was immunoprecipitated (IP) using an antibody against GATA-3, electrophoretically separated, and finally immunodetected using a Runx2 antibody (**c**, top panel). Levels of GATA-3 and phosphorylated (p)GATA-3 were immunodetected (middle panel). The amount of IgG heavy chains (IgG-H) was determined as the internal standard (bottom panel). The association of GATA-3 and Runx2 in MC3T3-E1 osteoblasts (Ob) was assayed as the positive control. These protein bands were quantified and statistically analyzed (**d**). Each value represents the mean $\pm$ s.e.m. for $n = 4$. * Values significantly differ from the respective control group, $P < 0.05$. d, day.

key initiating factors.[5] Our previous study has found that inflammation-induced oxidative stress stimulates the phosphorylation of p38 MAPK in osteoblasts and that activated p38 MAPK subsequently phosphorylates the downstream transcriptional factors nuclear factor-kappaB and activator protein-1.[36] Thus, one of the possible mechanisms explaining GATA-3 phosphorylation during fracture healing may be the activation of p38 MAPK, which is triggered by fracture-induced inflammation. The amount of nuclear GATA-3 was consecutively elevated during the healing of bone fractures. GATA-3 is a transcription factor that regulates the expression of multiple genes and consequently controls cell activities and functions.[15–17] As a result, bone healing is marked by the consecutive induction of GATA-3 mRNA and protein expression, as well as the phosphorylation and translocation of this transcriptional factor to the nucleus. Finally, activated GATA-3 may participate in osteoblast maturation and bone repair by adjusting the expression of certain genes.

Bcl-X_L participates in the process of bone healing by defending against fracture-induced insult. In parallel to healing,

expression of the bcl-x_L gene at the wound site was induced. Bcl-X_L, an antiapoptotic protein, is activated and translocated from the cytoplasm to the outer membranes of mitochondria, where it associates with the proapoptotic Bax and Bak proteins.[39] Bcl-X_L and Bcl-2 mediate survival signals and consequently protect osteoblasts from inflammation/oxidation-triggered programmed cell death.[12,40] When a fracture has occurred, fracture-induced inflammatory responses, including reactive oxygen species release, impaired perfusion and cell migration, are an important initiator that influences subsequent bone repair performance.[5] These inflammatory factors may result in osteoblast dysfunction or even apoptosis and may ultimately attenuate fracture healing. Huang et al.[41] have shown that overexpression of the bcl-x_L gene prevents cardiac cells from undergoing apoptosis by downregulating the translocation of the proapoptotic protein Bax and the release of cytochrome C. In addition, Bcl-xL has been reported to possess the novel cellular function of attenuating osteoclastic bone-resorption activity through downregulating the production of extracellular matrix proteins.[42] Therefore, Bcl-X_L plays crucial

Figure 7 GATA-3-mediated regulation of bcl-x_L gene expression during bone healing. Male ICR mice were anesthetized, and a metaphyseal bone defect was created in the left proximal femurs. The right femurs were treated as the sham group. At 1, 3, 5 and 7 days after surgery, the femurs were collected for the preparation of total RNA and genomic DNA. Levels of Bcl-X_L mRNA were analyzed using a reverse-transcription polymerase chain reaction (**a**, top panel). β-actin mRNA was measured as the internal standard (bottom panel). These DNA bands were quantified and statistically analyzed (**b**). A schematic diagram shows the GATA-3-specific DNA binding element (−463 to −471) and the positions of the forward and reverse primers designed for the chromatin immunoprecipitation (ChIP) assay in the promoter region of the bcl-x_L gene (**c**). The binding of GATA-3 to its specific DNA element in the promoter region of the bcl-x_L gene was determined using ChIP assays (**d**, top panel), and the inputs were used as the internal control (bottom panel). These DNA bands were quantified and statistically analyzed (**e**). Each value represents the mean ± s.e.m. for n = 4. * Values significantly (P < 0.05) differ from the respective control. d, day; M, DNA marker.

roles in stimulating fracture healing through decreasing inflammation-induced apoptotic insult or suppressing the bone resorption rate.

Runx2 contributes to the regulation of bone healing. Runx2 is an osteogenesis-related transcription factor that participates in osteoblast differentiation/mineralization and bone formation.[43] A previous study performed in our lab has shown that the Runx2 gene is induced during the progression of osteoblast protection against oxidative stress-induced cell apoptosis.[15] The present study complementarily provides in vivo evidence showing the augmentation of Runx2 mRNA and protein expression in the bone defect site during fractured bone healing. Runx2 has been demonstrated to be involved in fracture repair by controlling periosteal progenitor cell growth, differentiation and angiogenesis.[44] Moreover, the levels of nuclear Runx2 were significantly higher during bone healing.

Ho et al. have verified the roles of Runx2 in regulating expression of the bcl-2 gene, an antiapoptotic gene, and in successively contributing to NO protection against the oxidative stress-induced apoptosis of osteoblasts.[12] As a result, during the progression of bone healing, Runx2 may be induced at the transcriptional level, and subsequently participate in stimulating osteoblast differentiation/growth by regulating the expression of survival genes, such as Bcl-2 family proteins.

GATA-3 modulates bone healing via upregulating bcl-x_L gene expression, owing to its association with the Runx2 protein. The amounts of nuclear GATA-3 and Runx2 were considerably elevated at the insulted site. After phosphorylation, GATA-3 translocates into the nucleus from the cytoplasm and functions as a transcription factor.[12,16,17] Our current confocal microscopy imaging results showed the colocalization of GATA-3 and Runx2 in nuclei. Furthermore, protein signals

from co-immunoprecipitation and immunoblot assays showed the association of these two transcriptional factors. Our previous study has demonstrated the existence of such a GATA-3 and Runx2 complex in osteoblasts.[15] The present study revealed the specific expression of GATA-3 in recruited osteoblasts. Hence, GATA-3 and Runx2 are produced in osteoblasts ensconced in damaged bone sites, and these two transcriptional proteins may form a complex in nuclei. Dobreva et al.[45] have also reported the association of Runx2 with SATB2, a transcriptional factor that is a multifunctional determinant of osteoblast differentiation and craniofacial patterning. A biomedical approach has found the presence of the GATA-3-specific DNA-binding element (A/T)GATA(A/G) in the promoter region of the $bcl-x_L$ gene. Additionally, an electrophoretic mobility shift assay has also validated the binding of GATA-3 to its specific element in the $bcl-x_L$ promoter.[15] Knocking down GATA-3 translation using RNA interference simultaneously inhibits Bcl-X_L mRNA and protein expression by osteoblasts. Herein, we used a ChIP assay to show the transactivation activity of GATA-3 in regulating Bcl-X_L mRNA during bone healing. The present study provides an in vivo animal model to demonstrate that GATA-3 contributes to fracture healing by regulating $bcl-x_L$ gene expression on the basis of its association with Runx2.

In conclusion, this study showed the specific expression of GATA-3 in the bone defect area while fracture healing spontaneously occurred. Imaging analyses further revealed the co-localized expression of GATA-3 and ALP, thus indicating the production of GATA-3 by recruited osteoblasts. During the progression of bone healing, the levels of nuclear GATA-3 and pGATA-3 increased. In parallel, the amount of GATA-3 mRNA was induced during fracture healing. In addition, the expression of Runx2 mRNA and protein in the wounded area was significantly increased. Interestingly, analyses by confocal microscopy and co-immunoprecipitation demonstrated the association of nuclear GATA-3 and Runx2 during bone fracture healing. In parallel with fracture repair, expression of the $bcl-x_L$ gene was induced. Consequently, the results from the ChIP assay further showed the transactivation activity of GATA-3 in regulating $bcl-x_L$ gene expression. Thus, this translational study confirmed our previous in vitro findings regarding the roles of GATA-3 in regulating osteoblast survival/ death. Moreover, this study revealed the contributions of GATA-3 in guiding bone healing through upregulating $bcl-x_L$ gene expression to attenuate inflammation-induced insult. Our previous and present studies both show the beneficial roles of GATA-3 in maintaining osteoblast activities and bone healing. Therefore, GATA-3 may be clinically applied as a biomarker signature for the diagnosis and prognosis of bone diseases, such as bone fractures and osteoblast-induced fractures. In addition, GATA-3 has the potential to be an effective target for therapy of these bone diseases.

CONFLICT OF INTEREST
The authors declare no conflict of interest.

PUBLISHER'S NOTE
Springer Nature remains neutral with regard to jurisdictional claims in published maps and institutional affiliations.

1 Jepsen KJ, Silva MJ, Vashishth D, Guo XE, van der Meulen MC. Establishing biomechanical mechanisms in mouse models: practical guidelines for systematically evaluating phenotypic changes in the diaphyses of long bones. J Bone Miner Res 2015; 30: 951–966.
2 Rubin KH, Friis-Holmberg T, Hermann AP, Abrahamsen B, Brixen K. Risk assessment tools to identify women with increased risk of osteoporotic fracture: complexity or simplicity? A systematic review. J Bone Miner Res 2013; 28: 1701–1717.
3 Farrokhi MR, Alibai E, Maghami Z. Randomized controlled trial of percutaneous vertebroplasty versus optimal medical management for the relief of pain and disability in acute osteoporotic vertebral compression fractures. J Neurosurg Spine 2011; 14: 561–569.
4 Schindeler A, McDonald MM, Bokko P, Little DG. Bone remodeling during fracture repair: the cellular picture. Semin Cell Dev Biol 2008; 19: 459–466.
5 Pape HC, Marcucio R, Humphrey C, Colnot C, Knobe M, Harvey EJ. Trauma-induced inflammation and fracture healing. J Orthop Trauma 2010; 24: 522–525.
6 Reagan MR, Liaw L, Rosen CJ, Ghobrial IM. Dynamic interplay between bone and multiple myeloma: emerging roles of the osteoblast. Bone 2015; 75: 161–169.
7 Niedźwiedzki T, Filipowska J. Bone remodeling in the context of cellular and systemic regulation: the role of osteocytes and the nervous system. J Mol Endocrinol 2015; 55: R23–R36.
8 Lee RJ, Saylor PJ, Smith MR. Treatment and prevention of bone complications from prostate cancer. Bone 2011; 48: 88–95.
9 Sinder BP, Pettit AR, McCauley LK. Macrophages: their emerging roles in bone. J Bone Miner Res 2015; 30: 2140–2149.
10 Bai XC, Lu D, Liu AL, Zhang ZM, Li XM, Zou ZP et al. Reactive oxygen species stimulates receptor activator of NF-kappaB ligand expression in osteoblasts. J Biol Chem 2005; 280: 17497–17506.
11 Chen RM, Lin YL, Jean WC, Chen JS, Wang JH, Liu HC. Nitric oxide induces osteoblast apoptosis through the de novo synthesis of Bax protein. J Orthop Res 2002; 20: 295–302.
12 Ho WP, Chan WP, Hsieh MS, Chen RM. Runx2-mediated Bcl-2 gene expression contributes to nitric oxide protection against oxidative stress-induced osteoblast apoptosis. J Cell Biochem 2009; 108: 1084–1093.
13 Evans T, Felsenfeld G. The erythroid-specific transcription factor Eryf1: a new finger protein. Cell 1989; 58: 877–885.
14 Burch JB. Regulation of GATA gene expression during vertebrate development. Semin Cell Dev Biol 2005; 16: 71–81.
15 Chen RM, Lin YL, Chou CW. GATA-3 transduces survival signals in osteoblasts through upregulation of $bcl-x_L$ gene expression. J Bone Miner Res 2010; 25: 2193–2204.
16 Chen CH, Zhang DH, LaPorte JM, Ray A. Cyclic AMP activates p38 mitogen-activated protein kinase in Th2 cells: phosphorylation of GATA-3 and stimulation of Th2 cytokine gene expression. J Immunol 2000; 165: 5597–5605.
17 Furusawa J, Moro K, Motomura Y, Okamoto K, Zhu J, Takayanagi H et al. Critical role of p38 and GATA3 in natural helper cell function. Immunology 2013; 191: 1818–1826.
18 Kitagawa K, Shibata K, Matsumoto A, Matsumoto M, Ohhata T, Nakayama KI et al. Fbw7 targets GATA3 through cyclin-dependent kinase 2-dependent proteolysis and contributes to regulation of T-cell development. Mol Cell Biol 2014; 34: 2732–2744.
19 Hosokawa H, Tanaka T, Endo Y, Kato M, Shinoda K, Suzuki A et al. Akt1-mediated Gata3 phosphorylation controls the repression of IFNγ in memory-type Th2 cells. Nat Commun 2016; 7: 11289.

20 Meijome TE, Hooker RA, Cheng YH, Walker W, Horowitz MC, Fuchs RK et al. GATA-1 deficiency rescues trabecular but not cortical bone in OPG deficient mice. J Cell Physiol 2015; 230: 783–790.

21 Wu GJ, Wang W, Lin YL, Liu SH, Chen RM. Oxidative stress-induced apoptotic insults to rat osteoblasts are attenuated by nitric oxide pretreatment via GATA-5-involved regulation of Bcl-X$_L$ gene expression and protein translocation. Arch Toxicol 2016; 90: 905–916.

22 Hawse JR, Subramaniam M, Ingle JN, Oursler MJ, Rajamannan NM, Spelsberg TC. Estrogen-TGF-β cross-talk in bone and other cell types: role of TIEG, Runx2, and other transcription factors. J Cell Biochem 2008; 103: 383–392.

23 Yamaguchi M. Role of nutritional zinc in the prevention of osteoporosis. Mol Cell Biochem 2010; 338: 241–254.

24 Hsu YT, Wolter KG, Youle RJ. Cytosol-to-membrane redistribution of Bax and Bcl-X$_L$ during apoptosis. Proc Natl Acad Sci USA 1997; 94: 3668–3672.

25 Barnes GL, Kostenuik PJ, Gerstenfeld LC, Einhorn TA. Growth factor regulation of fracture repair. J Bone Miner Res 1999; 14: 1805–1815.

26 Uusitalo H, Rantakokko J, Ahonen M, Jämsä T, Tuukkanen J, KäHäri V et al. A metaphyseal defect model of the femur for studies of murine bone healing. Bone 2001; 28: 423–429.

27 Ho MH, Yao CJ, Liao MH, Lin PI, Liu SH, Chen RM. Chitosan nanofiber scaffold improves bone healing via stimulating trabecular bone production due to upregulation of the Runx2/osteocalcin/alkaline phosphatase signaling pathway. Intl J Nanomed 2015; 10: 5941–5954.

28 Lee YE, Liu HC, Lin YL, Liu SH, Yang RS, Chen RM. Drynaria fortunei J. Sm. improves the bone mass of ovariectomized rats through osteocalcin-involved endochondral ossification. J Ethnopharmacol 2014; 158: 98–104.

29 Lin JW, Chen JT, Hong CY, Lin YL, Wang KT, Yao CJ et al. Honokiol traverses the blood-brain barrier and induces apoptosis of neuroblastoma cells via an intrinsic Bax-mitochondrion-cytochrome c-caspase protease pathway. Neuro Oncol 2012; 14: 302–314.

30 Liao MH, Tai YT, Cherng YG, Liu SH, Chang YA, Lin PI et al. Genistein induces estrogen receptor-α gene expression in osteoblasts through activation of MAPKs/NF-κB/AP-1 and promotes cell mineralization. Br J Nutr 2014; 111: 55–63.

31 Yeh PS, Wang W, Chang YA, Lin CJ, Wang JJ, Chen RM. Honokiol induces autophagy of neuroblastoma cells through activating the PI3K/Akt/mTOR and endoplasmic reticular stress/ERK1/2 signaling pathways and suppressing cell migration. Cancer Lett 2016; 370: 66–77.

32 Farré D, Roset R, Huerta M, Adsuara JE, Roselló L, Albà MM et al. Identification of patterns in biological sequences at the ALGGEN server: PROMO and MALGEN. Nucleic Acids Res 2003; 31: 3651–3653.

33 Schug J. Using TESS to predict transcription factor binding sites in DNA sequence Current Protocols in Bioinformatics. Current Protocols: New Jersey, US, 2008. 2.6.1–2.6.15.

34 Li X, Kuang J, Shen Y, Majer MM, Nelson CC, Parsawar K et al. The atypical histone MacroH2A1.2 interacts with HER-2 protein in cancer cells. J Biol Chem 2012; 287: 23171–23183.

35 Damoulis PD, Hauschka PV. Nitric oxide acts in conjunction with proinflammatory cytokines to promote cell death in osteoblasts. J Bone Miner Res 1997; 12: 412–422.

36 Chen TL, Wu GJ, Hsu CS, Fong TH, Chen RM. Nitrosative stress induces osteoblast apoptosis through downregulating MAPK-mediated NFκB/AP-1 activation and subsequent Bcl-X$_L$ expression. Chem Biol Interact 2010; 184: 359–365.

37 Harvey NC, Glüer CC, Binkley N, McCloskey EV, Brandi ML, Cooper C et al. Trabecular bone score (TBS) as a new complementary approach for osteoporosis evaluation in clinical practice. Bone 2015; 78: 216–224.

38 Millán JL. The role of phosphatases in the initiation of skeletal mineralization. Calcif Tissue Int 2013; 93: 299–306.

39 Pagliari LJ, Kuwana T, Bonzon C, Newmeyer DD, Tu S, Beere HM et al. The multidomain proapoptotic molecules Bax and Bak are directly activated by heat. Proc Natl Acad Sci USA 2005; 102: 17975–17980.

40 Tai YT, Cherng YG, Chang CC, Hwang YP, Chen JT, Chen RM. Pretreatment with low nitric oxide protects osteoblasts from high nitric oxide-induced apoptotic insults through regulation of c-Jun N-terminal kinase/c-Jun-mediated Bcl-2 gene expression and protein translocation. J Orthop Res 2007; 25: 625–635.

41 Huang K, Nakamura K, Ito Y, Uzuka T, Morikawa M, Hirai S et al. Bcl-X$_L$ gene transfer inhibits Bax translocation and prolongs cardiac cold preservation time in rats. Circulation 2005; 112: 76–83.

42 Iwasawa M, Miyazaki T, Nagase Y, Akiyama T, Kadono Y, Nakamura M et al. The antiapoptotic protein Bcl-xL negatively regulates the bone-resorbing activity of osteoclasts in mice. J Clin Invest 2009; 119: 3149–3159.

43 Bruderer M, Richards RG, Alini M, Stoddart MJ. Role and regulation of RUNX2 in osteogenesis. Eur Cell Mater 2014; 28: 269–286.

44 Huang C, Xue M, Chen H, Jiao J, Herschman HR, O'Keefe RJ et al. The spatiotemporal role of COX-2 in osteogenic and chondrogenic differentiation of periosteum-derived mesenchymal progenitors in fracture repair. PLoS ONE 2014; 9: e100079.

45 Dobreva G, Chahrour M, Dautzenberg M, Chirivella L, Kanzler B, Fariñas I et al. SATB2 is a multifunctional determinant of craniofacial patterning and osteoblast differentiation. Cell 2006; 125: 971–986.